Single-particle dynamics of water molecules in confined space

M.-C. Bellissent-Funel,[1] S. H. Chen,[2] and J.-M. Zanotti[1]
[1]*Laboratoire Léon Brillouin, Commissariat à l'Energie Atomique–Centre National de la Recherche Scientifique, Centre d'Etudes de Saclay, 91191 Gif-sur-Yvette, France*
[2]*Department of Nuclear Engineering, Massachusetts Institute of Technology, Cambridge, Massachusetts 02139*
(Received 7 November 1994)

Recent neutron scattering studies of single-particle dynamics of water molecules contained in micropores of Vycor glass are presented. Results of incoherent quasielastic and inelastic neutron scattering spectra from the confined H_2O are analyzed to obtain the elastic incoherent structure factor, the short time self-diffusion constants, the residence time for jump diffusion, the rotational relaxation time, and the proton density of states as functions of coverage and temperature. Implication for the degree of confinement and slowing down of the single-particle motions are discussed in light of available NMR relaxation data and computer molecular dynamic simulation results.

PACS number(s): 61.25.−f, 68.45.−v

I. INTRODUCTION

The structural and dynamic properties of bulk water are now mostly well understood in some ranges of temperatures and pressures. In particular, many investigations using different techniques such as x-ray diffraction, neutron scattering, nuclear magnetic resonance (NMR), differential scanning calorimetry (DSC), molecular dynamics (MD), and Monte Carlo (MC) simulations have been performed in the deeply supercooled regime [1–8] and in a situation where the effects due to the hydrogen bonding are dominant.

In many common and relevant situations, water is not in its bulk form but instead attached to some substrates or filling small cavities. Common examples are water in porous media, such as rock or sand stones, and water in biological material as in the interior of cells or bound at the surface of biological macromolecules and membranes. This is what we define here as "confined water."

Water in confined space has attracted considerable interest in recent years. Understanding of the modification from bulk liquid water behavior when water is introduced into pores of porous media or confined in the vicinity of metallic surfaces is important to technological problems such as oil recovery from natural reservoirs, mining, heterogeneous catalysis, corrosion inhibition, and numerous other electrochemical processes. In particular, the assessment of perturbation of liquid water structure and dynamics by hydrophilic and hydrophobic molecular surfaces is fundamental to the quantitative understanding of the stability and enzymatic activity of globular proteins and functions of membranes. Water in porous materials such as Vycor glass, silica gel, and zeolites have been actively under investigation because of their relevance in catalytic and separation processes. Other examples of structures that impose spatial restriction on water molecules include polymer gels, clays, micelles, vesicles, and microemulsions. In the last three cases, since the hydrophobic effect is the primary cause for the self-organization of these structures, obviously the configuration of water molecules near the hydrophilic-hydrophobic interfaces is of considerable relevance.

In particular, the structure of water near layerlike clay minerals [9,10], polymeric membranes [11], and in various types of porous silica [12–17] has been studied by neutron diffraction. Also the structure of water confined in a hydrogel has been investigated by x-ray scattering [18] and the distortion seen at the level of the second nearest neighbors has been attributed to the bending of H bonds. Recently, the water-protein correlations at the surface of a fully deuterated amorphous protein C-Phycocyanin have been studied by neutron diffraction as functions of temperature and hydration level [19]. The correlation distance measured in these diffraction experiments compared well with computer simulations [20,21].

The dynamics of water molecules on the surface of C-Phycocyanin has also been studied recently using quasielastic and inelastic neutron scattering [22,23]. Previous studies about dynamics of water near interfaces by quasielastic neutron scattering involved measurements of the mobility of water on the surface of Nafion membranes [24,25], the diffusive motions and the density of states of water in silica gels [26], and the interfacial melting of ice in graphite and talc powders [27]. It is interesting to note that quasielastic-scattering–like effects for extremely small wave vectors can be observed in the pulsed gradient spin-echo NMR experiments; this technique has been used for studying diffusion of water in both permeable [28] and connected structures where the effects of confinement can be clearly identified [29].

An ideally microscopically detailed method for exploring the change in hydrogen-bonding patterns as well as the translational and rotational diffusion constants and residence times of water molecules, when they are near the surfaces, is computer molecular dynamics (CMD). For example, Rossky and co-workers [30–33] have investigated change of the structure, hydrogen-bonding, and dynamics of water molecules when they are adjacent to an atomically detailed hydrophobic surface and to a hydroxylated silica surface; Linse [34] made a similar

1063-651X/95/51(5)/4558(12)/$06.00

simulation for water near a charged surface with mobile counterions constituting an electric double layer such as in the interior of a reverse micelle formed with ionic surfactants in oil. These CMD results are still qualitative and somewhat conflicting with the available experimental data [35], largely because of the simplified models used for the surfaces and more certainly due to difficulties in choosing suitable potential functions for the simulations.

Traditionally, the dynamics of interfacial water has been studied by nuclear magnetic relaxation techniques. Halle and co-workers [36–38] have shown that oxygen-17 magnetic relaxation in water is dominated by quadrupolar coupling to the electric field gradient of the intramolecular origin. Thus it is a particularly suitable method for investigating single-particle dynamics of interfacial water of which the general findings are summarized below:

(a) perturbation (orientation and rotation) confined to water molecules in direct contact with surface;

(b) reorientation correlation time slows down by a factor of between 2 and 8 compared to the bulk water;

(c) reduced lateral mobility (factor of 10–100);

(d) long residence time in the first hydration shell (10–100 ps).

With regard to solvent diffusion constant near protein and silica surfaces there are reports from other groups that it is reduced by a factor of about 5 compared to bulk water [39,40].

Results of CMD simulations [30–34], [41–43] generally agreed that the dynamics of water molecules on protein and silica surfaces suffer only a mild slowing down compared to bulk water. More specifically, Rossky and Lee reported that the slowing down is by about a factor of 2 in the protein case and by about a factor of 5 in the silica case. Residence times of water in the first hydration layer are typically about 100 ps. Linse [34] also reported that water in the aqueous core of reverse micelles has a reduced rate of translational and rotational motions by a factor of 2–4.

From the above comparison it seems clear that there are considerable discrepancies in the degrees of slowing down between NMR experiments and CMD. This is especially true for the translational diffusion constant. We therefore have a strong motivation of performing neutron scattering experiments to resolve these discrepancies.

In the case of confined water it appears that we have to take into account two effects: the first one is due to the presence of a surface which can be either hydrophilic or hydrophobic; and the second one is due to the volume of confinement which can limit the extension of the hydrogen bond network in such a way as to reduce the density fluctuations of water. Thus, we expect to have significantly different transport properties of confined water. In order to separate the two effects, we studied water in a porous glass, Vycor, which is a model hydrophilic system, as a function of the level of hydration.

In previous papers [44,45] we have reported the results of a preliminary analysis of the incoherent quasielastic and inelastic neutron scattering of water in Vycor at several temperatures starting from the room temperature down to $-35\,^{\circ}\mathrm{C}$ and only for the case of half hydration (52%). In the present paper the results for several levels of hydration (full hydration, 52% and 25% hydration) in the same range of temperatures are presented.

II. THEORETICAL APPROACH TO MOTION OF WATER IN A CONFINED SPACE

A. Translational motion of water in a confined space

Since water is a triatomic, symmetric molecule, its single-particle dynamics consists of three components: vibrational, rotational, and translational motions. It is generally agreed in the literature that coupling between translational and rotational motions is weak and negligible. Under this assumption, as far as the quasielastic scattering is concerned, the intermediate scattering function is a product of three factors, each representing the component motion. A detailed discussion of the intermediate scattering function for bulk water, which is an infinite medium, and its extension to the case of confined water has been given in Ref. [8]. For a translationally invariant system, the van Hove self-correlation function $G_S(r,t)$ is a function of a scalar distance r and time. The intermediate scattering function $F_S(Q,t)$ can be derived from the self-correlation function $G_S(r,t)$ by a three-dimensional Fourier transform

$$F_S(Q,t)=\int e^{i\mathbf{Q}\cdot\mathbf{r}}G_S(r,t)d^3r \ . \tag{1}$$

However, an imposition of a confinement breaks the translational symmetry and the van Hove self-correlation function is no longer a function of a scalar variable r but is instead a function, $G_S(\mathbf{r}_0,\mathbf{r},t)$, which depends on both the test particle position $\mathbf{r}$ at time t and its initial position $\mathbf{r}_0$ at time zero. In this latter case the intermediate scattering function has to be calculated according to a double integral

$$F_S(Q,t)=\int e^{i\mathbf{Q}\cdot(\mathbf{r}-\mathbf{r}_0)}G_S(\mathbf{r}_0,\mathbf{r},t)p(\mathbf{r}_0)d^3r_0d^3r \ . \tag{2}$$

The intermediate scattering function is still a function of a scalar Q because of a powder average one makes for an isotropic sample.

In Eq. (2), $p(\mathbf{r}_0)$ is the equilibrium distribution function of the test particle under the confining potential. It is easy to see that Eq. (2) reduces to Eq. (1) for the case of an infinite medium, like a bulk liquid. In this special case $p(\mathbf{r}_0)$ is independent of the position and equals an inverse of the sample volume. $G_S(\mathbf{r}_0,\mathbf{r},t)$ is now a function of $|\mathbf{r}-\mathbf{r}_0|$ due to the translational symmetry. So the integration on the initial position can be carried out which cancels the volume factor.

Since the van Hove self-correlation function is a conditional probability of finding the test particle at $\mathbf{r}$ at time t, given that the particle was at $\mathbf{r}_0$ at time zero, there are three general properties the function has to satisfy:

(i) the normalization of the probability

$$\int G_S(\mathbf{r}_0,\mathbf{r},t)p(\mathbf{r}_0)d^3r_0d^3r=1 , \tag{3}$$

(ii) the initial condition

$$G_S(\mathbf{r}_0,\mathbf{r},0)=\delta(\mathbf{r}-\mathbf{r}_0) , \tag{4}$$

(iii) the approach to a stationary distribution

$$G_S(\mathbf{r}_0,\mathbf{r},\infty)=p(\mathbf{r})=\frac{1}{Z}\exp\left[-\frac{V(r)}{k_BT}\right] , \tag{5}$$

where Z is a normalization factor defined in such a way that the volume integral of $p(\mathbf{r})$ for all space is unity.

The simplest model for the translational motion of a water molecule in a confined space is diffusion of a point particle inside a sphere of radius a. This belongs to a class of general problems of diffusion of a particle in a potential field $V(r)$ and is describable by the Smoluchowsky equation. The partial differential equation for a particle in a spherically symmetric potential $V(r)$ is of the form

$$\frac{1}{D}\frac{\partial G_S}{\partial t}=\frac{1}{r^2}\frac{\partial}{\partial r}\left[r^2\frac{\partial G_S}{\partial r}+\frac{1}{k_BT}r^2\frac{dV}{dr}G_S\right]-\frac{\hat{L}^2}{r^2}G_S , \tag{6}$$

where D is the diffusion constant of the particle and $\hat{L}^2$ is the operator for the square of the angular momentum. Volino and Dianoux [46] solved this equation for a potential $V(r)$ which is zero everywhere inside a sphere of radius a and is infinity outside the sphere. The intermediate scattering function defined in Eq. (2) can be written in the form

$$F_S(Q,t)=\sum_{l=0}^{\infty}(2l+1)\sum_{n=0}^{\infty}A_n^l(Q)\exp[-\lambda_n^l t] , \tag{7}$$

where λ_n^l is the (l,n)th eigenvalue of a one-dimensional steady-state Schrödinger-like equation, derived from the Smoluchowsky equation (6), and which is necessarily real and non-negative since the van Hove correlation function is positive, real, and finite. The amplitude factor $A_n^l(Q)$ is the Fourier transform of the eigenfunctions of the equation.

The first term in Eq. (7) is a constant in time because the lowest eigenvalue $\lambda_0^0=0$. This is derived from the fact that the van Hove self-correlation function for a particle confined by a potential does not decay to zero at infinite time but instead approaches a stationary distribution as given by Eq. (5). This fact alone immediately leads to the existence of an elastic component in the dynamic structure factor. In fact the amplitude factor corresponding to the lowest eigenvalue is given by

$$A_0^0(Q)=\left|\int p(r)e^{i\mathbf{Q}\cdot\mathbf{r}}d^3r\right|^2=\left|\frac{1}{V}\int_v e^{i\mathbf{Q}\cdot\mathbf{r}}d^3r\right|^2 . \tag{8}$$

The second equality comes about because $p(r)$ is equal to 1 over the volume inside the confining volume and zero outside. This Q-dependent amplitude factor is called the elastic incoherent structure factor (EISF) and is identical to the form factor of the confining volume V. We give analytical expressions of the EISF for two geometries:

(i) sphere of a radius a,

$$A_0^0(Qa)=\left[\frac{3j_1(Qa)}{Qa}\right]^2 ; \tag{9}$$

(ii) cylinder of height L and cross-sectional radius a,

$$A_0^0(Qa)=\int_0^1 d\mu[j_0(QL\mu/2)]^2\left[\frac{2J_1(Qa\sqrt{1-\mu^2})}{Qa\sqrt{1-\mu^2}}\right]^2 . \tag{10}$$

Since $F_S(Q,0)=1$ from the definition Eq. (2) and the property Eq. (4), we have a sum rule

$$\sum_{l=0}^{\infty}(2l+1)\sum_{n=0}^{\infty}A_n^l(Q)=1 . \tag{11}$$

This means that the EISF, which is the first term of Eq. (11), is the fractional elastic intensity of all the modes.

The self-dynamic structure factor as measured by an incoherent quasielastic neutron scattering is the time Fourier integral of the intermediate scattering function given in Eq. (7). It is

$$S_S(Q,\omega)=A_0^0(Q)\delta(\omega)+\frac{1}{\pi}\sum_{\{l,n\}\neq\{0,0\}}(2l+1)A_n^l(Q)\times\frac{(x_n^l)^2D/a^2}{\omega^2+[(x_n^l)^2D/a^2]^2} , \tag{12}$$

where $x_n^l=a\sqrt{\lambda_n^l/D}$ are dimensionless numbers and the values of the first 99 of them were tabulated by Volino and Dianoux [46].

As can be seen from Eq. (12), there is an elastic peak with a fractional intensity $A_0^0(Q)$ and a series of Lorentzian quasielastic lines, each with a fractional intensity $A_n^l(Q)$. Figure 1, taken from Ref. [46], shows the relative intensities of the first nine modes. In practice one gets an elastic peak and a combined quasielastic Lorentzian line with a width depending on the values of diffusion constant D and radius a. The Q dependence of this quasielastic linewidth is plotted in Fig. 2.

It is useful to observe here that the most important effect of confinement is the appearance of an elastic mode with a substantial intensity at low Q. In fact, at $Q=0$ there is only the elastic mode and it continues to dom-

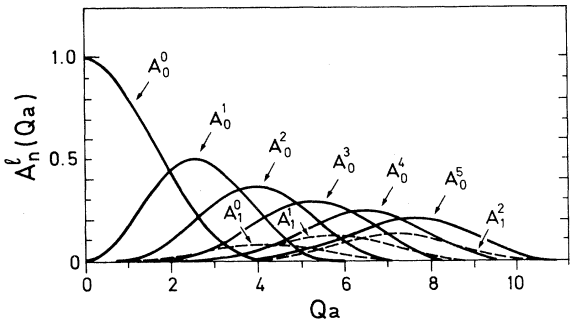

FIG. 1. Variation of the first nine incoherent structure factors vs Qa for a particle diffusing inside a sphere of radius a. The EISF is $A_0^0(Q)$. (Figure taken from Ref. [46].)

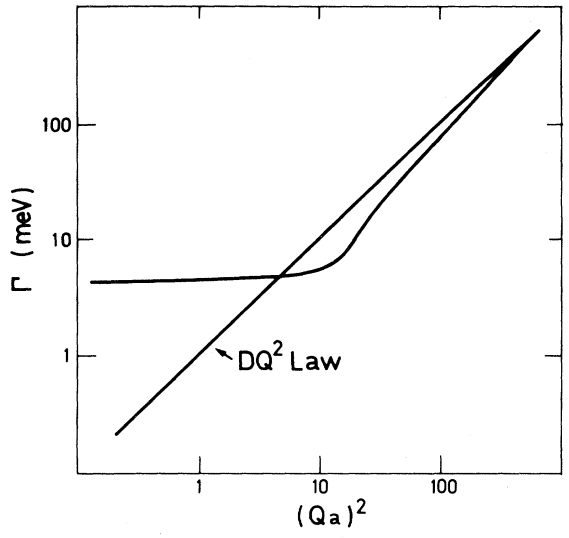

FIG. 2. Variation of the linewidth (half width at half maximum) Γ of the quasielastic line vs $(Qa)^2$ for a particle diffusing inside a sphere of radius a. Γ is given in units of D/a^2. As a comparison, the case for free diffusion is also shown. (Figure taken from Ref. [46].)

inate the total intensity up to $Qa=1$. At $Qa=4$ the elastic intensity vanishes, and beyond that there are only quasielastic lines. In a typical quasielastic neutron scattering (QENS) spectrometer, the maximum Q is about 2 Å^{-1}, and taking $a=5$ Å, the product is 10. Looking at Fig. 1, we see that for data in this Q range the first ten modes contribute to the intensity. We now turn our attention next to the quasielastic linewidth. Figure 2 shows that the half width at half maximum Γ of the quasielastic line is practically constant and equals to $4.33D/a^2$ from $Qa=0$ until $Qa=3.3$. But in practical terms for $Qa<1$ the intensity of the quasielastic line is vanishingly small and one has nearly pure elastic scattering. For $Qa>3.3$, the intensity of the elastic peak goes to zero and one is left with a quasielastic line, the Γ of which nearly follows the macroscopic diffusion law DQ^2.

In practice, one cannot really distinguish between different quasielastic lines, so it is expedient to simply put the intermediate scattering function for the translational motion as

$$F_S^t(Q,t)=A_0^0(Q)+[1-A_0^0(Q)]e^{-\Gamma_t(Q)t} \tag{13}$$

and the corresponding self-dynamic structure factor as

$$S_S^t(Q,\omega)=A_0^0(Q)\delta(\omega)+[1-A_0^0(Q)]L_1(\omega,\Gamma_t)\ , \tag{14}$$

where $L_1(\omega,\Gamma_t)$ denotes a Lorentzian function of an argument ω and a half width at half maximum Γ_t.

Extension of the theory to the case of diffusion inside a volume with an anisotropic shape, such as a cylinder having a height L and a cross-sectional radius a, has been given by Dianoux, Pineri, and Volino [47]. In this case the natural length scale of the problem is $\rho=(a^2+L^2/4)^{1/2}$. The EISF is given by Eq. (10) which is the form factor of a cylinder. The EISF plotted in terms of a nondimensional scale $Q\rho$ shows a broader peak with considerably enhanced Q tail, especially for a larger axial ratio $\delta=L/2a$. Again at low Q the quasielastic linewidth is practically constant, having a value

$$\Gamma=\lambda(\delta)D/\rho^2\ , \tag{15}$$

where $\lambda(\delta)$ is a function of δ, varying between 2.5 and 5.8, with the highest value occurring at $\delta=1$. The range of constant Γ is about $0<Q\rho<4$ for the axial ratio $0.1<\delta<2$.

B. Vibrational motion of water in a confined space

The vibrational part of the intermediate scattering function is just a Debye-Waller factor resulting from the finite amplitude of the vibrational motions of the hydrogen atoms [8]. This factor is $\exp[-\langle u^2\rangle Q^2/3]$. The mean-square vibrational amplitude of hydrogen atoms in water at room temperature was determined to be [48] $\langle u^2\rangle=0.152$ Å^2, so in the Q range of the measurements the factor is nearly unity and in the data fitting process it was taken to be unity.

C. Rotational motion of water in a confined space

The rotational part of the intermediate scattering function was computed using a rotational approximation [8]. In this approximation it is written

$$F_S^R(Q,t)=j_0(Qb)^2+3j_1(Qb)^2\exp(-2D_rt)+5j_2(Qb)^2\exp(-6D_rt)+\cdots\ . \tag{16}$$

In the Q range of the measurements the amplitudes of the third and higher order terms are negligible. As the result, the corresponding dynamic structure factor is approximated as

$$S_S^R(Q,\omega)=B_0(Q)\delta(\omega)+[1-B_0(Q)]L_2(\omega,\Gamma_r)\ , \tag{17}$$

where $B_0(Q)=j_0(Qb)^2$ and $\Gamma_r=2D_r$.

D. Single-particle dynamic structure factor of water in a confined space

The complete single-particle dynamic structure factor of water is a convolution of dynamic structure factors for the translational and rotational motions [see Eq. (18)]. This equation is the result of assuming that translational and rotational motions are decoupled. The justification of this assumption has already been discussed in several papers [49–51]. In a recent paper [48] we have analyzed the bulk water data, according to this decoupled model, and found it fits all the data remarkably well and the extracted parameters Γ_t and Γ_r can be interpreted in a rather consistent manner,

$$S_S(Q,\omega)=S_S^t(Q,\omega)\otimes S_S^R(Q,\omega)\ , \tag{18}$$

where $\otimes$ means convolution in ω. In particular, there is an elastic peak with an EISF given by

$$A_0(Q)=\left[\frac{3j_1(Qa)}{Qa}\right]^2 j_0(Qb)^2\ . \tag{19}$$

In water b is the O—H bond length which is 1 Å. The confining radius turns out to be about 5 Å at room temperature. Thus the second factor in the EISF is relatively unimportant compared to the first one for the Q range of interest.

III. PROTON DENSITY OF STATES

As mentioned in a previous work [8], the Q-dependent density of states of the H atom is given by

$$G_S(Q,\omega)=\frac{M_{H_2O}}{k_BT}\left[\frac{\hbar\omega}{Q}\right]^2\exp\left[-\frac{\hbar\omega}{k_BT}\right]S_S(Q,\omega)\ . \quad (20)$$

It can be shown that in an isotropic liquid, the above-defined function approaches a genuine density of states $f_H(\omega)$ as Q tends to zero, namely,

$$\lim_{Q\to 0} G_S(Q,\omega)=f_H(\omega)\ . \quad (21)$$

In practice, for water, the Q tends to zero condition is satisfied for $Q<3$ Å^{-1}. This condition can be met for the lowest angle detector bank in the MIBEMOL spectrometer.

IV. EXPERIMENT

The quasielastic and inelastic neutron scattering experiments were performed at Laboratoire Léon Brillouin using a MIBEMOL high-resolution time-of-flight spectrometer. In order to separate the translational and the rotational components in the spectra, identical measurements were made with two different resolutions, one high and the other low. Using the MIBEMOL spectrometer, the high-resolution runs have a full width at half maximum

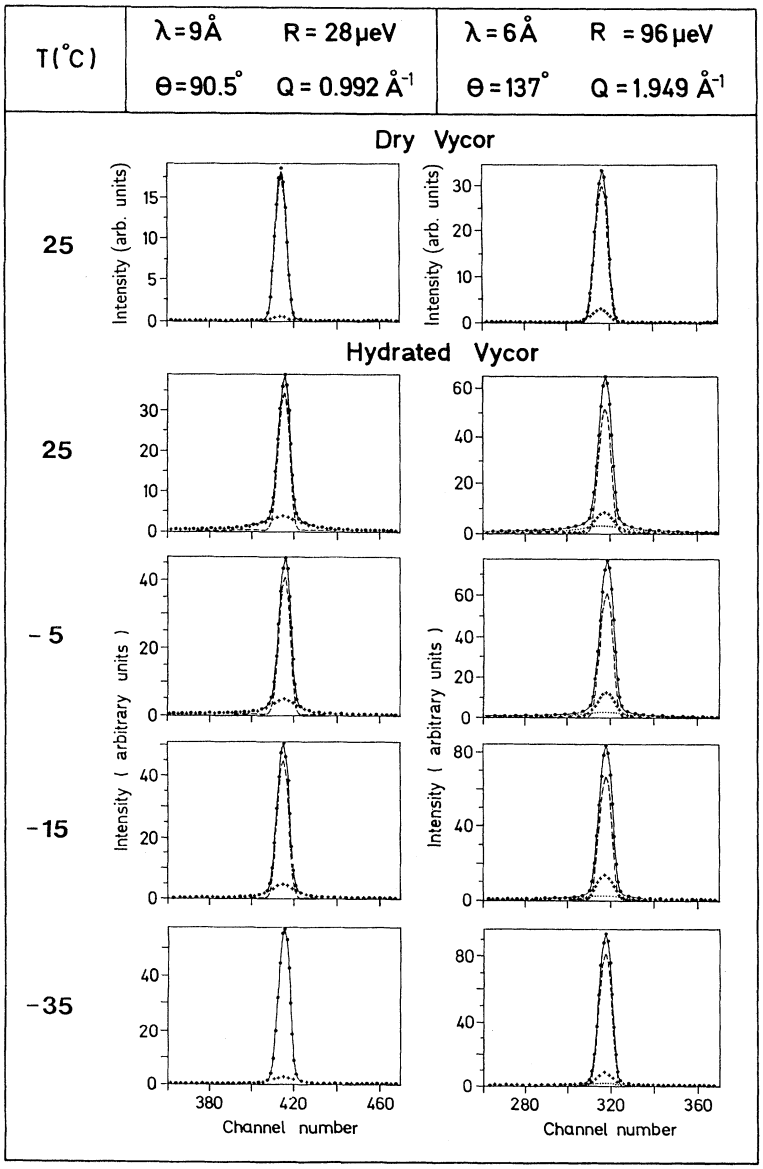

FIG. 3. Typical spectra from a quasielastic neutron scattering experiment on 25% hydrated (with H_2O) Vycor. Points are the measurements and solid lines are the model fits. Notice the spectra generally consist of resolution broadened elastic and quasielastic peaks.

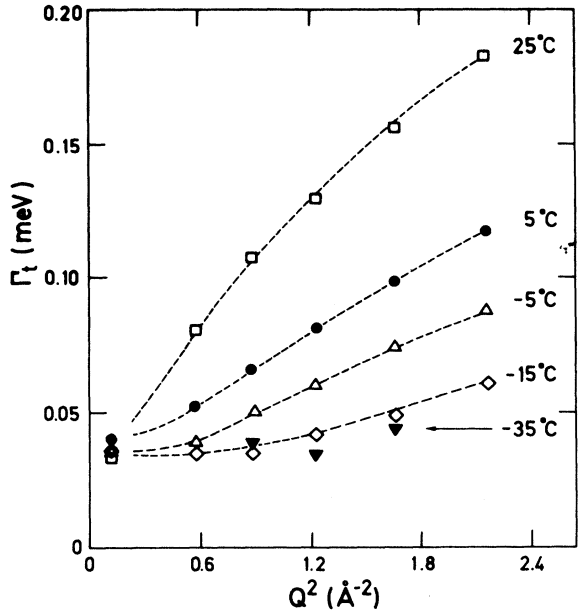

FIG. 4. Restricted translational linewidth Γ_t of water contained in 100% hydrated Vycor plotted as a function of Q^2 for five temperatures: 25, 5, −5, −15, and −35 °C. We see that there is some evidence of a plateau at −5 and −15 °C.

(R) of 28 μ eV, and the low-resolution runs have an R of 96 μ eV. The wave-vector ranges covered, respectively, in the two resolutions were from 0.21 to 1.28 Å^{-1} for the high-resolution runs (using 9-Å neutrons) and from 0.32 to 1.93 Å^{-1} for the low-resolution runs (using 6-Å neutrons).

Vycor brand porous glass No. 7930 is a product of Corning Glass Works. Vycor glass is made by heating a homogeneous mixture of boron oxide glass and silica glass above the melting point and then quenching this mixture to a temperature below the spinodal line where the mixture phase separates into two mutually interpenetrating regions. At a certain stage of preparation, the boron rich region is leached out by acid, leaving behind a silica skeleton with a given distribution of pore sizes. We used rectangular plate samples, the thickness of which was 1.6 mm and the area 32×36 mm^2. The average pore size of Vycor 7930 is 50 Å, as stated by the manufacturer [52].

We adopted the following procedure for the preparation of the Vycor samples. The rectangular plates of Vycor were immersed in 30% hydrogen peroxide and heated to 90 °C for a few hours to remove any organic impurities absorbed by the glass. The Vycor was then washed several times in distilled water in order to remove the hydrogen peroxide and stored in distilled water. When a hydrated Vycor sample is heated at 90 °C in vacuum till dry, it becomes translucent and clear, defining what we called a "dry Vycor sample." At full hydration, a Vycor glass absorbs water up to 25% of its dry weight. A partially hydrated sample is then obtained by absorption of water in the vapor phase until the desired level of hydration is reached. The sample we used in this experiment was hydrated to a level of 52% and 25%. Based on the information that the dry density of Vycor is 1.45 g/ml, the porosity 28%, and the internal cylindrical pores of cross-sectional diameter 50 Å, the 52% hydrated sample has 3 to 4 layers of water on its internal surface. In order to achieve a monolayer coverage, a 25% hydrated sample has been prepared.

V. MODEL FOR ANALYSIS

We use the following simplified models for the analysis of the quasielastic scattering data. First of all, we analyzed data from a dry Vycor sample which scatters neutrons coherently with a cross section of few barn and thus ten times lower than the scattering cross section of H_2O which is mainly incoherent and about 160 b; we found out that the spectra of Vycor consisted of an elastic line which can be represented by a delta function with a constant area A that is Q independent. For partially hydrated Vycor, on the other hand, there is evidence of both elastic and inelastic lines. We found that the elastic line consists of two components, one with a Q-independent amplitude and the other with a Q-dependent amplitude. We assume that the Q-independent one is due to the elastic scattering of Vycor itself. Thus a model scattering law for the high-resolution experiment (using 9-Å neutrons) can be written as

$$S_h(Q,\omega)=A\delta(\omega)+x\{B(Q)\delta(\omega)+[1-B(Q)]L_1(\omega,\Gamma_t)\}+\mathcal{B}\ , \tag{22}$$

where the spectrum given by the second term represents the translational component of the scattering law of wa-

TABLE I. Extracted parameters for 100% hydrated Vycor. (Our estimate of error bars can be as high as 30% for the values of D_{local} at 25 °C.)

T (°C)	a (Å)	D_{local} Confined $\left[10^{-5}\frac{\text{cm}^2}{\text{s}}\right]$	D_t Confined $\left[10^{-5}\frac{\text{cm}^2}{\text{s}}\right]$	D Bulk $\left[10^{-5}\frac{\text{cm}^2}{\text{s}}\right]$	τ_0 Confined (ps)	τ_0 Bulk (ps)
25			2.43	2.30	2.2	1.10
5	5.0	3.30	1.43	1.30	2.3	2.33
−5	4.5	2.53	1.01	0.907	2.7	4.66
−15	3.5	1.41	0.75	0.574	4.3	8.90

ter molecules which consists of an elastic line with a fractional area $B(Q)$ and a quasielastic line represented by a Lorentzian function with a line width Γ_t, having a fractional area $1-B(Q)$. The relative area of the spectrum due to Vycor and of the spectrum due to water is set equal to A/x. We added further a constant background term $\mathcal{B}$. The scattering law $S_h(Q,\omega)$ was then convolved with the instrumental resolution function. This analytical form fits all the data at 9 Å very well for all the temperatures. We extracted the Q-dependent elastic fraction $B(Q)$, and the narrow quasielastic linewidth Γ_t. From the low-resolution data taken at 6 Å, we were able to extract an additional broader line width Γ_r by imposing the known narrow linewidth Γ_t obtained from the high-resolution data. Thus the scattering law we used for the analysis of the low-resolution data is as follows:

$$S_l(Q,\omega)=A\delta(\omega)+x\{B(Q)\delta(\omega)+[1-B(Q)]L_1(\omega,\Gamma_t)\}\otimes\{C(Q)\delta(\omega)+[1-C(Q)]L_2(\omega,\Gamma_r)\}+\mathcal{B}\,. \tag{23}$$

In the second term of this scattering law, the first factor represents the translational component and the second factor the rotational component of water molecules.

This scattering law $S_l(Q,\omega)$, when convolved with the instrumental resolution function, again fits the 6-Å data quite well. The quality of the fit for data for the 25% hydrated sample is illustrated in Fig. 3.

VI. RESULTS AND DISCUSSION

A. 100% hydrated sample

Figure 4 gives the translational linewidth Γ_t extracted from measurements using the MIBEMOL spectrometer with incident neutrons having an average wavelength of 8 Å. At this wavelength, energy resolution of the instrument is 50 μ eV (FWHM). The reliable Q range is from 0.35 to 1.47 Å^{-1}. Γ_t is plotted as a function of Q^2 for five temperatures: 25, 5, −5, −15, and −35 °C. As the temperature decreases from 25 °C, Γ_t versus Q^2 curves at first show a flat and constant value Γ_0 at small Q. Then they increase and asymptotically approach another constant values Γ_∞ at large Q. The first feature is due to the confinement effect and can be approximately accounted for by the model of Volino and Dianoux [46]. The latter model predicts that the plateau value Γ_∞ persists until $Q=Q_0$ at a level $4.33[D_{\text{local}}/a^2]$ with $Q_0=\pi/a$. The localization radius a can be deduced from fitting the Q

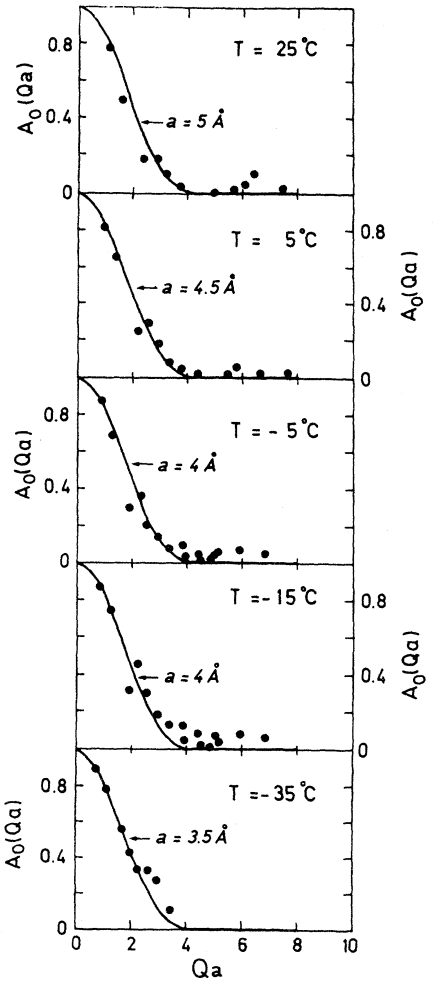

FIG. 5. The elastic incoherent structure factor $A_0(Qa)$ for water contained in 52% hydrated Vycor obtained from analysis of 9-Å and 6-Å data for four temperatures: 25, 5, −5, and −15 °C. The last $A_0(Qa)$ at −35 °C is from 9-Å data. Solid circles are the data and solid lines are the best fits using Eq. (19).

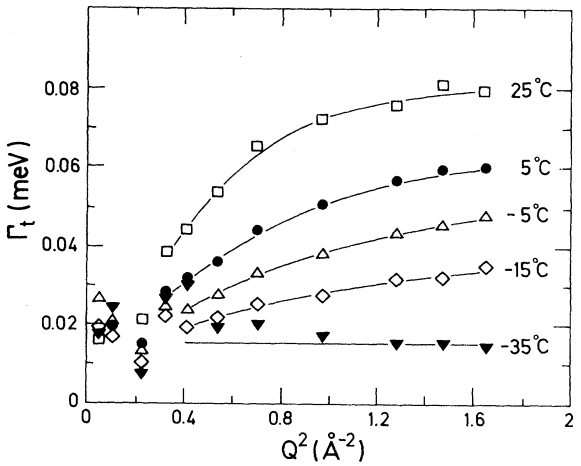

FIG. 6. Restricted translational linewidth Γ_t of water contained in 52% hydrated Vycor plotted as a function of Q^2 for the five temperatures given in the last figure. The symbols are obtained from analysis of 9-Å data for which the energy resolution (half width at half maximum) is equal to 14 μeV. We see that there is a definite evidence of the initial plateau extending up to $Q^2=0.4$ Å^{-2}, which is about 20 μeV. Solid lines are model fits to high Q data using jump diffusion model Eq. (24).

TABLE II. Extracted parameters for 52% hydrated Vycor. (Our estimate of error bars can be as high as 30% for the values of D_{local} at 25 °C.)

T (°C)	a (Å)	D_{local} Confined $\left[10^{-5}\frac{\text{cm}^2}{\text{s}}\right]$	D_t Confined $\left[10^{-5}\frac{\text{cm}^2}{\text{s}}\right]$	τ_0 Confined (ps)	τ_0 Bulk (ps)	τ_1 Confined (ps)	τ_1 Bulk (ps)
25	5	1.76	2.61	5.7	1.10	1.03	1.10
5	4.5	1.42	1.82	7.8	2.33	1.36	1.38
−5	4	1.12	1.29	9.7	4.66	1.52	1.57
−15	4	1.12	1.19	16	8.90	1.80	1.92
−35	3.5			44			

dependence of the extracted EISF. Values of the localization radius decrease slowly when the temperature decreases, indicating that water molecules become more confined at lower temperatures. At larger Q values, the linewidths follow the well-known jump diffusion behavior [8] given by

$$\Gamma_t(Q)=\frac{D_tQ^2}{1+D_tQ^2\tau_0}\ , \tag{24}$$

where τ_0 represents the residence time before jump and D_t the short-time translational diffusion constant. The values of D_t and τ_0 are deduced respectively from the slope and the intercept of the linear variation of the curve $1/\Gamma_t$ as a function of $1/Q^2$. The values of D_t and τ_0 deduced from data shown in Fig. 4 are given in Table I. The diffusion coefficient within the confinement volume D_{local} has been estimated from the limit of the translational linewidth at small Q values. It is smaller than the diffusion constant in bulk water. The determination of D_{local} is difficult at room temperature, but possible at lower temperatures where the effect of confinement becomes more apparent.

B. 52% hydrated sample

Figure 5 gives the extracted EISF as a function of Q at different temperatures. One sees that the theoretical EISF given in Eq. (19) fits the data reasonably well. In order to get better fits to the tail part of the curves, a cylindrical confining volume, as given in Eq. (10), may be needed. But the statistical accuracy of the data does not warrant such an undertaking. The radii of confining volume starts out at 5 Å at room temperature and decreases slowly as the temperature goes down, reaching 3.5 Å at −35 °C. The case of −35 °C is anomalous due to the presence of some amount of cubic ice in water [53]. The trend that water molecules are progressively more localized at low temperatures is reasonable.

Figure 6 gives the translational linewidth Γ_t extracted from the high-resolution measurements for the 52% hydrated sample. It is plotted as a function of Q^2 for five temperatures: 25, 5, −5, −15, and −35 °C. The reliable Q range is from 0.47 to 1.28 Å^{-1}. At the lowest temperature, the linewidth saturates at 0.015 meV, close to the limit of the instrumental resolution (halfwidth =0.014 meV). It is seen that at larger Q, the linewidths tend to flatten out indicating a jump diffusion behavior [8]. The residence time τ_0 increases rapidly as the temperature decreases, as seen from Table II. At −15 °C, for example, it is 16 ps.

According to the model of Volino *et al.*, the linewidth Γ_0 in the zero Q limit should remain at a finite value. Our linewidth data are not very reliable for Q smaller than 0.47 Å^{-1}. However, at 25 °C the value of the local diffusion coefficient D_{local} is estimated to be equal to 1.76×10^{-5} cm^2 s^{-1}. This is within a factor of 2 smaller than the known value of the diffusion constant of bulk water [48]. On the other hand, a preliminary spin-echo NMR experiment [54] revealed that values of the diffusion coefficient measured this way are much smaller than the neutron ones. This is due to the fact that the

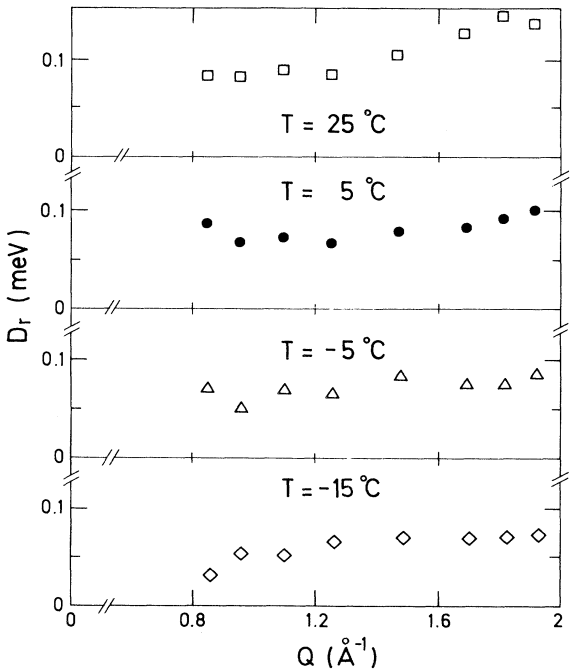

FIG. 7. Half of the rotational linewidth D_r extracted from low-resolution data plotted as a function of Q for four temperatures. These curves show that within the statistical error of the fitted parameters, D_r is independent of Q.

NMR technique measures a long time translational diffusion coefficient. These latter findings are in agreement with the diffusional behavior of water confined in Nafion membranes [24,25], where some evidence of local and long range diffusion has been shown.

The data from the low-resolution runs were treated by including both Lorentzian functions $L_1(\omega,\Gamma_t)$ and $L_2(\omega,\Gamma_r)$ as mentioned earlier. In these fittings, the translational linewidths are treated as known values. The extracted Γ_r, or half of it, called the rotational diffusion constant D_r, is shown in Fig. 7. One can see that the rotational diffusion constants are independent of Q as they should be. Table II summarizes the relevant Q-independent parameters extracted from our QENS experiments. The rotational relaxation time $\tau_1 = 1/6D_r$ is

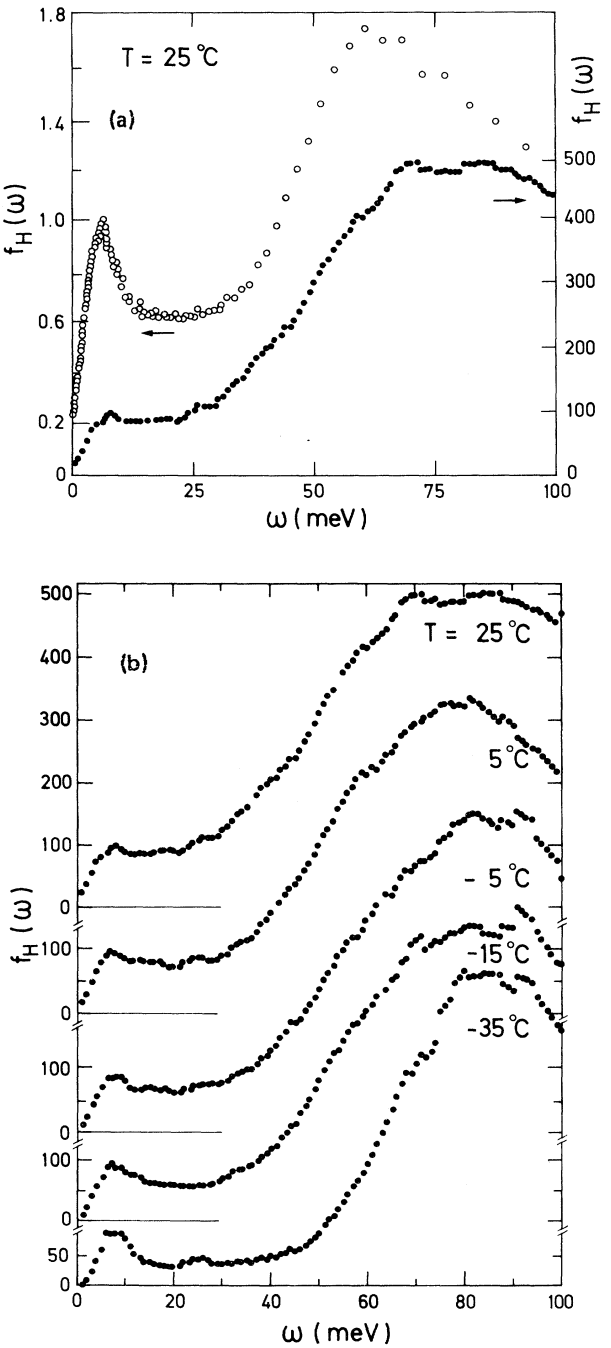

FIG. 8 (a) Proton density of states for water contained in 52% hydrated Vycor at 298 K (solid circles). For comparison the corresponding quantity for bulk water (open circles) is also given. (b) Evolution of the proton density of states for water contained in 52% hydrated Vycor as a function of the temperature.

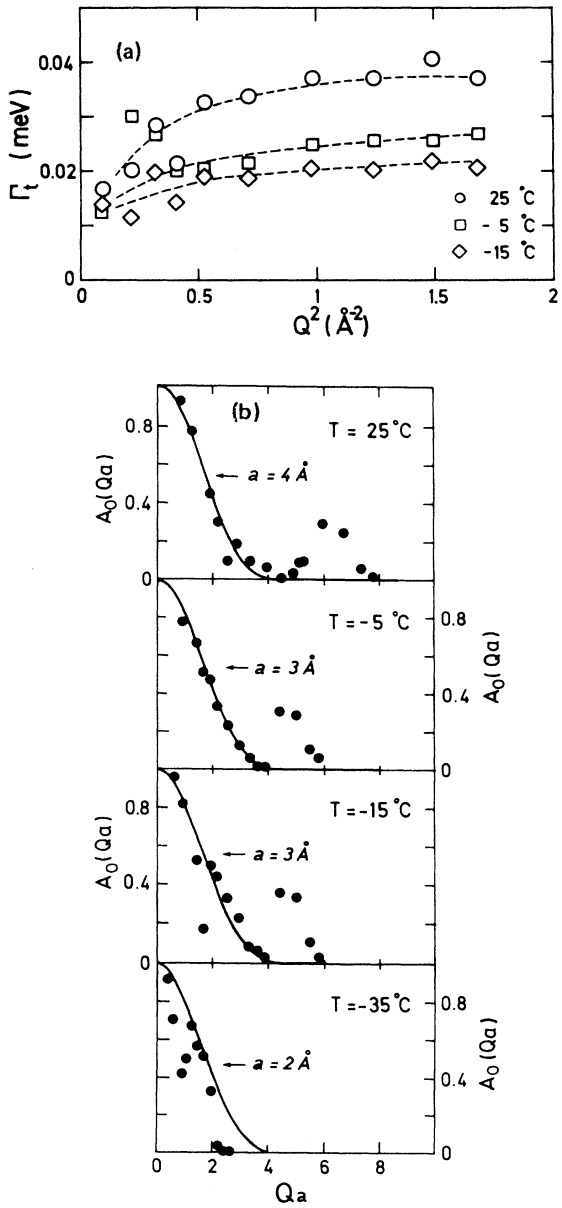

FIG. 9. (a) Restricted translational linewidth Γ_t of water contained in 25% hydrated Vycor plotted as a function of Q^2 at three temperatures: 25, −5, and −15 °C. (b) The elastic incoherent structure factor $A_0(Qa)$ for water contained in 25% hydrated Vycor obtained from analysis of 9-Å and 6-Å data for four temperatures: 25, −5, −15, and −35 °C. Solid circles are the data and solid lines are the best fits using Eq. (19).

TABLE III. Extracted parameters for 25% hydrated Vycor. (Our estimate of error bars can be as high as 30% for the values of D_{local} at 25 °C.)

T (°C)	a (Å)	D_{local} Confined $\left[10^{-5}\frac{\text{cm}^2}{\text{s}}\right]$	D_t Confined $\left[10^{-5}\frac{\text{cm}^2}{\text{s}}\right]$	τ_0 Confined (ps)	τ_0 Bulk (ps)	τ_1 Confined (ps)	τ_1 Bulk (ps)
25	4	0.92	2.45	15	1.10	1.5	1.10
−5	3	0.38	1.36	20	4.66	1.8	1.57
−15	3	0.26	1.20	25	8.90	2.0	1.92
−35	2					3.1	

given alongside the residence time for jump diffusion, τ_0. Experimental values for bulk water at the same temperature [8] are also given for comparison. It is clear from Table II that while the residence time for jump diffusion shows substantial slowing down upon confinement, the rotational relaxation time which is associated with the hydrogen bond lifetime remains nearly the same as in bulk water.

Figure 8(a) shows the proton density of states for both the confined water (52% hydrated Vycor) (lower curve) and bulk water (upper curve) at room temperature. Striking features of the density of states of the confined water are a much attenuated peak associated with the translational motions, centered around 6 meV, indicating the reduction of this degree of freedom upon confinement; and an upshift of the librational peak at 70 meV, signifying hindrance of the librational motions by the presence of a surface. Figure 8(b) gives the evolution of the density of states for confined water as a function of temperature. The upshift of the librational peak increases as the temperature is lowered which reflects the amplified effect of confinement.

C. 25% hydrated sample

In order to obtain a monolayer of water molecules on the internal surface of Vycor, we made a 25% hydrated sample, according to our best estimate. As in the previous cases we made measurements using two different wavelengths, namely, 9 Å and 6 Å. The translational linewidth Γ_t extracted from the high-resolution measurements is plotted as a function of Q^2 for three temperatures: 25, −5, and −15 °C in Fig. 9(a). The same characteristics as obtained for the 100% and 52% hydrated samples were observed: a finite value Γ_0 of the translational linewidth at low Q values and flattening out of this width at high Q values. The extracted EISF are plotted in Fig. 9(b) for the three temperatures. They are reasonably fitted with an EISF for a spherical localization volume whose radius varies between 4 and 2 Å. Table III gives values of D_{local}, D_t, τ_0, and τ_1 extracted from the data and the corresponding values of τ_0 and τ_1 for bulk water. The values obtained for D_{local} are low compared to D_t which demonstrates the influence of the hydrophilic groups on the water molecules when one reaches a monolayer coverage. Moreover, D_{local} so obtained are close to values of the diffusion coefficient of water molecules at the immediate vicinity of a hydrophililc interface as determined in a recent MD simulation by Lee and Rossky [33]. We are thus able to discriminate the effect of the substrate. On the other hand, values of D_t and τ_1 are very close to that of bulk water while values of τ_0 are much higher. Figures 10(a) and 10(b) give, respectively, the Arrhenius plots of τ_0 and τ_1 for bulk water and for water in Vycor at different levels of hydration.

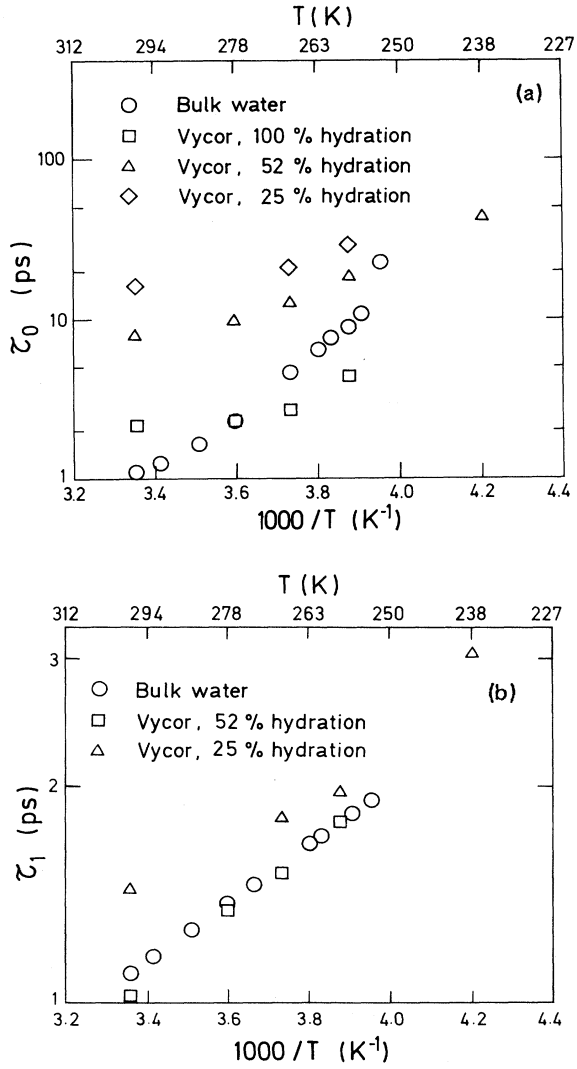

FIG. 10. (a) Arrhenius plot of the residence time τ_0 for confined water as compared with bulk water. (b) Arrhenius plot of the hindered rotations characteristic time, τ_1. This last time can be associated with the hydrogen-bond lifetime.

VII. CONCLUSION

In this paper we have described the short time diffusion (less than 40 ps) of water molecules close to a hydrophilic silica surface in terms of a simple model. Samples studied have levels of hydration in the range between 100% and 25%, the latter corresponding to a monolayer coverage of water molecules on the surface. The effect of temperature has been followed from the room temperature down to $-35\,^{\circ}C$.

A spherical volume of confinement approximately accounts for the EISF. The radius of the sphere varies between 5 and 2 Å. It decreases as the temperature is lowered. The trend that the water molecules are more localized at lower temperatures seems reasonable.

From the small Q part of the quasielastic linewidth, a diffusion constant in the localization volume has been deduced and is defined as D_{local}. For the 100% hydrated sample the value of D_{local} at a given temperature is close to the corresponding value for the translational diffusion constant of the bulk water. For the 52% and 25% hydrated samples the values of D_{local} decrease when the level of hydration or the temperature decrease. In particular for the 25% hydrated sample $D_{\text{local}}=0.92\times10^{-5}$ cm^2/s at 25 °C and is in agreement with MD simulations of Lee and Rossky [33].

The Q dependence of the large Q part of the quasielastic linewidth is well accounted by a jump diffusion model. The fitted values of the diffusion coefficient D_t are close to values found for the bulk water whatever the level of hydration and are always slightly higher. The residence time τ_0 of confined water is always longer than the residence time of bulk water at the same temperature. For example, for the 25% hydrated sample $\tau_0=25$ ps at $-15\,^{\circ}C$.

The values of the hydrogen-bond lifetime τ_1 are very close to that of the values for bulk water and vary between 1.1 and 3.0 ps. Analogous to bulk water, the hydrogen-bond lifetime τ_1 for confined water has an Arrhenius temperature dependence while the residence time τ_0 does not exhibit such a behavior.

To conclude, at short time, water molecules close to a hydrophilic surface perform very local rotational jumps characterized by D_t and τ_1 like in bulk water, but with a longer residence time on a given site before diffusing to an adjacent site along the surface with a diffusion coefficient equal to D_{local}. This diffusion is confined to a volume estimated as spherical in shape.

For the 52% hydrated sample the diffusion coefficient measured by a NMR experiment appears to be smaller than D_{local} which is in turn smaller than D_t. That is due to the fact that these diffusion coefficients in confined space are time-dependent quantities. The NMR technique measures a long time and long range diffusion coefficient for which the relevant confinement volume is larger.

The proton density of states for confined water corresponding to the 52% hydrated sample shows a shift in the bending mode and the librational mode to higher frequencies which means that the intermolecular motions of water molecules close to a hydrophilic surface are hindered. The hindrance of the motions increases when the temperature is lowered. In particular there is an attenuation of the bending mode of confined water. We expect this mode to disappear for the 25% hydrated sample. New incoherent inelastic neutron scattering experiments are being planned as a function of the temperature and for low hydrated samples to study the intermolecular density of states of confined water. We also are contemplating a very-high-resolution quasielastic neutron scattering experiment combined with a new NMR experiment.

ACKNOWLEDGMENTS

Research of S.H.C. is supported by a grant from the Material Sciences Division of U.S. DOE. We are grateful to NATO for financial support that made this research collaboration possible. M.-C.B.F. acknowledges J.R.C. van der Maarel for his participation in the NMR experiments and for his hospitality at the laboratory in Leiden during the course of the NMR experiments.

[1] C. A. Angell, in *Water: A Comprehensive Treatise,* edited by F. Franks (Plenum, New York, 1981), Vol. 7, Chap. 1.
[2] E. W. Lang and H. D. Ludemann, Angew. Chem. Int. Ed. Engl. **21**, 315 (1982).
[3] S. H. Chen and J. Teixeira, Adv. Chem. Phys. **64**, 1 (1985).
[4] J. C. Dore, in *Water Science Reviews,* edited by F. Franks (Cambridge University Press, Cambridge, 1985), Vol. 1.
[5] M.-C. Bellissent-Funel, J. Teixeira, and L. Bosio, J. Chem. Phys. **87**, 2231 (1987).
[6] M.-C. Bellissent-Funel, in *Hydrogen-Bonded Liquids,* Vol. 329 of *NATO Advanced Study Institute, Series C: Mathematical and Physical Sciences,* edited by J. C. Dore and J. Teixeira (Kluwer Academic, Dordrecht, 1991).
[7] M.-C. Bellissent-Funel and J. Teixeira, J. Mol. Struct. **250**, 213 (1991).
[8] S. H. Chen, in *Hydrogen-Bonded Liquids* (Ref. [6]), p. 289.
[9] R. K. Hawkins and P. A. Egelstaff, Clays Clay Miner. **28**, 19 (1980).
[10] A. K. Soper, in *Hydrogen-Bonded Liquids* (Ref. [6]), p. 147.
[11] P. M. Wiggins, Prog. Polym. Sci. **13**, 1 (1988).
[12] D. C. Steytler and J. C. Dore, J. Chem. Phys. **87**, 2458 (1983).
[13] D. C. Steytler, J. C. Dore, and C. J. Wright, Mol. Phys. **48**, 1031 (1983).
[14] D. C. Steytler and J. C. Dore, Mol. Phys. **5**, 1001 (1985).
[15] J. C. Dore, M. Dunn, and P. Chieux, J. Phys. (Paris) Colloq. **48**, C1-457 (1987).
[16] J. C. Dore, F. Coveney, and M.-C. Bellissent-Funel, *Recent Developments in the Physics of Fluids,* edited by W. S.

Howells and K. Soper (Hilger, London, 1992), p. 299.
[17] M. J. Benham, J. C. Cook, J. C. Li, A. D. K. Ross, P. L. Hall, and B. Sarkissian, Phys. Rev. B **39**, 633 (1989).
[18] L. Bosio, G. P. Johari, M. Oumezzine, and J. Teixeira, Chem. Phys. Lett. **188**, 113 (1992).
[19] M.-C. Bellissent-Funel, J. Lal, K. F. Bradley, and S. H. Chen, Biophys. J **64**, 1542 (1993).
[20] P. J. Rossky and M. Karplus, J. Am. Chem. Soc. **101**, 1913 (1979).
[21] M. Levitt and R. Sharon, Proc. Natl. Acad. Sci. U.S.A. **85**, 7557 (1988).
[22] M.-C. Bellissent-Funel, J. Teixeira, K. F. Bradley, S. H. Chen, and H. L. Crespi, Physica B **180&181**, 740 (1992).
[23] M.-C. Bellissent-Funel, J. Teixeira, K. F. Bradley, and S. H. Chen, J. Phys. I France **2**, 995 (1992).
[24] F. Volino, M. Pineri, A. J. Dianoux, and A. de Geyer, J. Polym. Sci. **20**, 481 (1982).
[25] A. J. Dianoux, in *The Physics and Chemistry of Aqueous Ionic Solutions,* Vol. 205 of *NATO Advanced Study Institute, Series C: Mathematical and Physical Sciences,* edited by M.-C. Bellissent-Funel and G. W. Neilson (Reidel, Dordrecht, 1987), p. 147.
[26] J. D. F. Ramsay and C. Poinsignon, Langmuir **3**, 320 (1987).
[27] M. Maruyama, M. Bienfait, J. G. Dash, and G. Coddens, J. Cryst. Growth **118**, 33 (1992).
[28] P. T. Callaghan, A. Coy, T. P. J. Halpin, D. Mac Gowan, K. J. Packer, and F. O. Zelaya, J. Chem. Phys. **97**, 651 (1992).
[29] P. T. Callaghan, A. Coy, D. Mac Gowan, K. J. Packer, and F. O. Zelaya, Nature **351**, 467 (1991).
[30] C. Y. Lee, J. A. McCammon, and P. J. Rossky, J. Chem. Phys. **80**, 4448 (1984).
[31] S. H. Lee and P. J. Rossky, in *Proceedings of the 10th Korean Scientists and Engineers Conference* (Inchen, Korea, 1987), p. 150.
[32] P. J. Rossky and S. H. Lee, Chem. Scr. **29A**, 93 (1989).
[33] S. H. Lee and P. J. Rossky, J. Chem. Phys. **100**, 3334 (1994).
[34] P. Linse, J. Chem. Phys. **90**, 4992 (1989).
[35] L. Piculell and B. Halle, in *Water and Aqueous Solutions,* edited by G. W. Neilson and J. E. Enderby (Hilger, Bristol, 1986), and references therein.
[36] B. Halle, T. Andersson, S. Forsen, and B. Lindman, J. Am. Chem. Soc. **103**, 500 (1981).
[37] B. Halle and G. Carlstroem, J. Phys. Chem. **85**, 2142 (1981).
[38] G. Carlstroem and B. Halle, Langmuir **4**, 1346 (1988).
[39] C. F. Polnazek, D. A. Hanggi, P. W. Carr, and R. G. Bryant, Anal. Chim. Acta. **194**, 311 (1987).
[40] C. F. Polnazek and R. G. Bryant, J. Am. Chem. Soc. **106**, 428 (1984); J. Chem. Phys. **81**, 4038 (1984).
[41] W. F. van Gunsteren, H. J. C. Berendsen, and J. Hermans, J. Mol. Biol. **176**, 559 (1984).
[42] C. F. Wong and J. A. McCammon, Isr. J. Chem. Phys. **27**, 211 (1986).
[43] P. Ahlstrom, O. Teleman, and B. Johnson, J. Am. Chem. Soc. **110**, 4198 (1988).
[44] M.-C. Bellissent-Funel, K. F. Bradley, S. H. Chen, J. Lal, and J. Teixeira, Physica A **201**, 277 (1993).
[45] S. H. Chen and M. C. Bellissent-Funel, in *Hydrogen Bond Networks,* Vol. 435 of *NATO Advanced Study Institute, Series C: Mathematical and Physical Sciences,* edited by M. C. Bellissent-Funel and J. C. Dore (Kluwer Academic, Dordrecht, 1994), p. 307.
[46] F. Volino and A. J. Dianoux, Mol. Phys. **41**, 271 (1980).
[47] A. J. Dianoux, M. Pineri, and F. Volino, Mol. Phys. **46**, 129 (1982).
[48] J. Teixeira, M.-C. Bellissent-Funel, S. H. Chen, and A. J. Dianoux, Phys. Rev. A **31**, 1913 (1985).
[49] S. Yip, *Spectroscopy in Biology and Chemistry, Neutron, X-ray, Laser,* edited by S. H. Chen and S. Yip (Academic, New York, 1974), Chap. 2.
[50] A. Rahman and F. H. Stillinger, J. Chem. Phys. **55**, 3336 (1971).
[51] A. Rahman and F. H. Stillinger, J. Chem. Phys. **57**, 1281 (1972).
[52] General information on Vycor Brand Porous "thirsty glass," No. 7930, Corning Glass Works, is available from OEM Sales Service, Box 5000, Corning, NY 14830, USA.
[53] M.-C. Bellissent-Funel, J. Lal, and L. Bosio, J. Chem. Phys. **98**, 4246 (1993).
[54] M.-C. Bellissent-Funel and J. R. C. van der Maarel (unpublished).